Geophysical Research Letters

RESEARCH LETTER
10.1029/2021GL092414

Key Points:

- Cusp auroral intensity is essentially determined by solar wind power input related to the interplanetary magnetic field (IMF) magnitude, IMF direction, and solar wind speed
- Auroral midday gaps are predominantly observed under southward IMF, implying that cusp aurora is statistically weak during the southward IMF
- The IMF B_y magnitude plays a key role in determining the cusp aurora intensity, although the solar wind speed also contributes

Correspondence to:
D.-S. Han,
handesheng@tongji.edu.cn

Citation:
Qiu, H.-X., Han, D.-S., Feng, H.-T., Shi, R., Zhou, S., & Zhang, Y.-L. (2021). The critical factor in controlling the auroral intensity in the cusp region as revealed by a statistical study on midday gap and non-gap events. *Geophysical Research Letters*, *48*, e2021GL092414. https://doi.org/10.1029/2021GL092414

Received 5 JAN 2021
Accepted 19 MAR 2021

The Critical Factor in Controlling the Auroral Intensity in the Cusp Region as Revealed by a Statistical Study on Midday Gap and Non-Gap Events

Hui-Xuan Qiu[1], De-Sheng Han[1], Hui-Ting Feng[1], Run Shi[1], Su Zhou[2], and Y.-L. Zhang[3]

[1]State Key Laboratory of Marine Geology, School of Ocean and Earth Science, Tongji University, Shanghai, China, [2]School of Electronics and Communication Engineering, Guiyang University, Guiyang, China, [3]The Johns Hopkins University Applied Physics Laboratory, Laurel, MD, USA

Abstract Taking advantage of the high spatial-resolution and global coverage of Defense Meteorological Satellite Program/Special Sensor Ultraviolet Spectrographic Imager observations, we investigated the critical interplanetary factors in controlling the cusp auroral emission by dividing the midday auroras into the gap (weak emission) and non-gap (intense emission) events. Although the cusp auroral intensity is essentially determined by a parameter related to the IMF (interplanetary magnetic field) direction, IMF magnitude ($|B_y|$), and solar wind speed (V), we found that the cusp aurora is statistically weak during the southward IMF but intense when the V and IMF $|B_y|$ are greater. Further, we confirmed that even with $V > 600$ km/s, the intense-aurora event still shows a minimum occurrence near the IMF $|B_y| = 0$. However, when the IMF $|B_y|$ is greater, the V becomes less significant for the intense-aurora occurrence. These results demonstrate that the IMF $|B_y|$ is critical in controlling the cusp auroral intensity, most likely by producing an electric field which is given as $V \times B_y$.

Plain Language Summary The solar wind carries the IMF throughout the solar system, which interacts with the earth's magnetic field and results in the magnetosphere. The polar cusp is a particular region of the magnetosphere where the solar wind particles can directly enter the upper atmosphere and thus produce aurora. The IMF can be decomposed into, B_x, B_y, and B_z components that are in the Earth-to-Sun, eastward, and northward directions, respectively. It has been well recognized that the solar wind power input to the magnetosphere is more significant under the southward IMF (negative B_z) condition. Therefore, one generally expects that the auroral intensity in the cusp region should be more intense under the southward IMF condition. In this work, we found that the cusp auroral intensity is statistically weak during the southward IMF condition, which is apparently not expected. The statistical results indicate that the IMF $|B_y|$ is critical in controlling the cusp auroral intensity.

1. Introduction

The polar cusp is a funnel-shaped region of the dayside magnetosphere, which extends downward from the high-altitude magnetopause to the polar ionosphere and corresponds to the auroral oval in the midday sector (Frank et al., 1971; Heikkila & Winningham, 1971; Russell et al., 1998). Using auroral photographs from the Defense Meteorological Satellite Program (DMSP), Snyder and Akasofu (1976) noticed that the midday sector of the auroral oval is a "permanent" gap, which has been called the "auroral midday gap." The auroral midday gap was suggested to be the cusp's optical signature (Meng, 1981), and several studies on the midday gap have been carried out (Dandekar, 1979; Dandekar & Pike, 1978).

Later, it was noticed that the midday gap is not permanent because the ground-based instruments (Eather et al., 1981) and satellite imagers (Meng & Lundin, 1986; Zhang et al., 2005) frequently observed "non-gap" events, that is, full of the aurora, in this sector. The gap is always observed in the midday sector, indicating that the auroral intensity in this region is generally weak. When the auroral intensity cannot reach the sensitivity threshold of the instruments, a "gap" is observed.

Despite the average intensity being early noticed to be weak, the auroras in the cusp region have been extensively studied. Based on the ground-based optical observations, the auroras observed in the cusp region

have been classified into different types, and their dependencies on the interplanetary conditions have been extensively studied (e.g., Sandholt, 1997). The electrons for producing the cusp auroras were confirmed directly from the magnetosheath and accelerated by dispersive Alfvén waves (Mende et al., 2016). Poleward moving auroral forms (PMAF) were often observed in this region as the signature of flux transfer events (Fasel et al., 1995), and their dynamical evolution was found to be well controlled by the IMF (interplanetary magnetic field) B_y component (e.g., Moen et al., 1998). As for the cusp auroral intensity, Fuselier et al. (2002) noticed that a broad and intense cusp emission might be developed by a cusp spot merging into the auroral oval as the IMF turns from the northward to the southward. Trondsen et al. (1999) found that the auroral oval was observed to be intense and continuous throughout the cusp region for negative IMF B_y. Yang et al. (2013) suggested that the enhanced solar wind speed was vital to the dayside aurora intensification. Based on ground observations, Hu et al. (2012) indicated that the midday aurora intensity showed a good correlation with a northward solar wind electric field produced by $V \times B_y$, where V is solar wind speed. Newell et al. (2009, 2010) systematically examined the global auroral precipitations (including the cusp region) varied with season and the solar wind driving by using DMSP particle observations. However, among all of the factors mentioned above, which factor is critical in controlling the auroral intensity in the cusp region is still unclear.

In this study, taking advantage of the high spatial-resolution and global coverage of the auroral observations from the Special Sensor Ultraviolet Spectrographic Imager (SSUSI) on DMSP, we conducted a detailed study on the midday aurora. The statistical results, for the first time, clearly show the vital role of the IMF B_y magnitude in determining the cusp auroral intensity.

2. Data Set and Event Selection

The DMSP spacecraft have been operating since 1965 at an altitude of about 840 km in polar sun-synchronous orbits with a 101-min orbital period and 98.9° orbital inclination (Hardy et al., 2008; Ober et al., 2014). SSUSI is designed to sense the ionosphere and thermosphere remotely by providing horizon-to-horizon images at five wavelengths, including HI (121.6 nm), OI (130.4 nm), OI (135.6 nm), N_2 (LBHS, 140–150 nm), and N_2 (LBHL, 165–180 nm). For each orbit, the DMSP/SSUSI produces two images that cover part of the auroral oval in the Northern and Southern Hemispheres, respectively. Compared with previous satellite-based observations on aurora, the DMSP/SSUSI has the advantages of high spatial-resolution and long-term continuous observation. The DMSP satellites began carrying the SSUSI instrument in 2003. We used the observations from 2013 to 2017 only in the Northern Hemisphere. The IMF and solar wind data are taken from NASA/GSFC's OMNI data set through the CDAWeb.

In this study, we plot LBHS observations of DMSP/SSUSI in MLT-MagLat (geomagnetic latitude) coordinates with a latitudinal range of 50°–90° and with a unified emission scale of 0.05–5.0 kR. All of the gap and non-gap events are visually selected from these images based on if the auroral intensity is less or greater than 0.3 kR, respectively, as shown in Figure 1. Figure 1a shows an example of the midday gap event observed on January 25, 2017. The red dotted lines indicate the duskward and dawnward edges, which indicate the gap approximately spans from 1000 to 1400 MLT. Figure 1b is a non-gap example observed on November 08, 2017, which shows that the midday sector is filled with aurora. Figures 1c and 1d present the IMF and solar wind conditions corresponding to the midday gap and non-gap events shown in Figures 1a and 1b, respectively. Generally, the satellite needs to fly ~ 25 min to produce such an image. The UT time shown on the image is the start time of the satellite recording the image.

Based on the criteria shown in Figure 1, we selected 8267 gap events and 5740 non-gap events from the available DMSP F16, F17, and F18 observations from 2013 to 2017. In this study, we only used the typical gap and non-gap events but discarded all the ambiguous ones. The advantage of this method is successful classification of the cusp auroras into two classes, namely weak (gap) and intense (non-gap) cases, by taking the auroral emissions in the whole cusp region into account. This advantage is important in evaluating the key factors in determining the cusp auroral intensity.

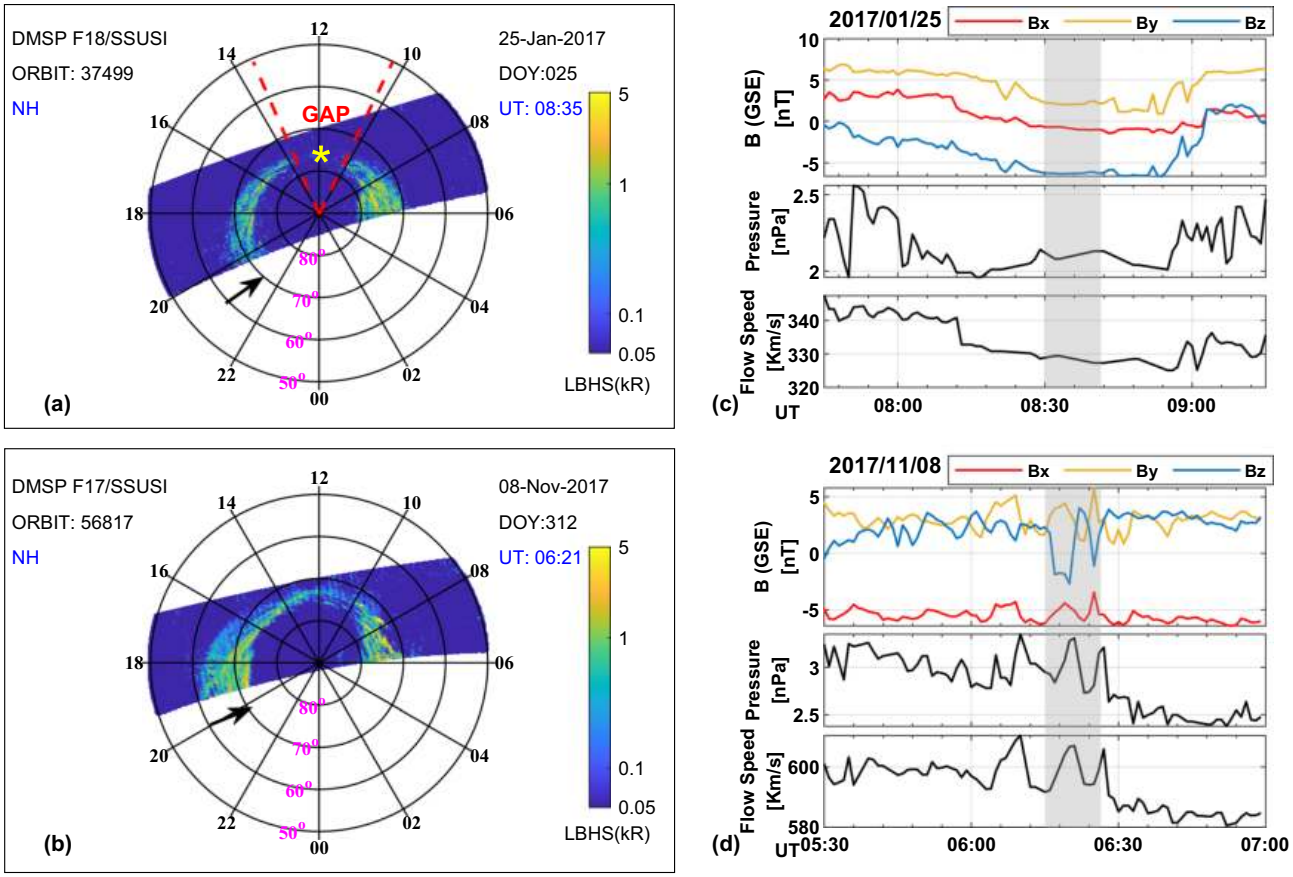

Figure 1. (a) and (b) Typical examples of the midday gap and non-gap events, respectively. The corresponding IMF and solar wind conditions are shown in (c) and (d), respectively. The auroral observations have been mapped into MLT-MagLat (geomagnetic latitude) coordinates. The satellite (DMSP F18/F17), orbit number (ORBIT), hemisphere information (NH: Northern Hemisphere), observation date, day of the year (DOY), and the start time of the image (UT) are given on the image. The black arrow indicates the forward direction of the satellite. The right panels show the IMF (B_x, B_y, and B_z), dynamic pressure, and solar wind flow speed from top to bottom. The gray area indicates the time period for calculating the parametric mean value in this study.

3. Statistical Results

3.1. The Apparent Differences of the Gap and Non-Gap Events Dependent on the Interplanetary Conditions

First, we investigated the dependencies of the midday gap and non-gap events on the interplanetary conditions by comparing their occurrence conditions with a background condition. The occurrence condition is 10-min averaged OMNI data taken from −5 to +5 min of the satellite passing through 1200 MLT by considering a 5-min time delay from the OMNI observation at the magnetopause to the ionospheric response. The background conditions are 15,000 averaged values of 10-min OMNI data randomly selected from 2013 to 2017 which is the same period of already selected gap and non-gap events. In Figure 2, the blue and yellow bars present the distributions of occurrence conditions for the midday gap and non-gap events on the interplanetary conditions, respectively. The gray bars show the distributions of the background condition. For the interplanetary conditions, we selected the IMF B_x, B_y, B_z, IMF clock angle ($\theta = \arctan(B_y/B_z)$), solar wind speed (V), solar wind dynamic pressure, solar wind density, and a parameter of $d\Phi_{MP}/dt$. Here, $d\Phi_{MP}/dt = v^{4/3}B_T{}^{2/3}\sin^{8/3}(\theta/2)$, which is a parameter that best predicts the global solar wind power input to the magnetosphere (Newell et al., 2007, 2009). Besides showing the event distribution, we simply estimated the occurrence rates of the gap and non-gap events by dividing the event number by the background number for each bin. The blue and yellow curves with dots show the relative occurrence rates of the gap and non-gap events, respectively, which shows apparent differences between the gap and non-gap events in all of the parameters.

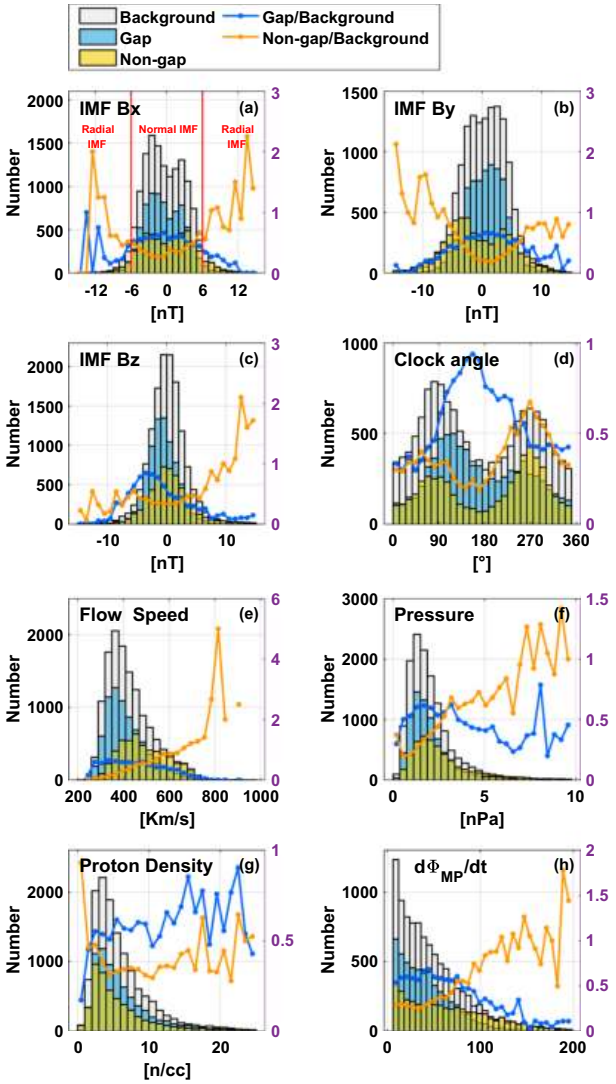

Figure 2. The statistical distributions of the IMF and solar wind conditions of the midday gap events (blue bars), non-gap events (yellow bars), and the background (gray bars). The blue and yellow curves with dots show the relative occurrences of the gap and non-gap events, respectively.

The statistical results shown in Figure 2 are summarized as follows.

1. For the gap events, the distributions of occurrence and background conditions (as shown by the blue and gray bars) are quite similar, except for the IMF B_z biased toward negative. Please note that it is just this bias that leads to a high occurrence of the gap event from 90° to 270° clock angle, as shown in Figure 2d.
2. For the non-gap events, we see that the distributions of the IMF B_y and the solar wind speed show apparent differences from the background distributions. The B_y effect can be clearly seen in Figure 2b by comparing the distributions for the gap and non-gap events. The distribution of the non-gap events shows two peaks at high $|B_y|$ values. However, the gap events are clustered at one peak centered near $B_y = 0$ nT.
3. Comparing the occurrence rates of gap and non-gap events, we see that the larger $|B_x|$, larger $|B_y|$, positive B_z, ~90° and ~270° clock angle, high solar wind speed, high dynamic pressure, low solar wind density, and high solar wind power input are favorable to the non-gap event occurrence.
4. Especially, Figure 2h shows that when the solar wind power input, that is, the value of $d\Phi_{MP}/dt$, is low, the occurrence rate of the gap event is higher than that of the non-gap event. When the $d\Phi_{MP}/dt$ value becomes high, the occurrence rate of the non-gap event is apparently larger than that of the gap event. These indicate that the cusp auroral intensity is essentially controlled by the solar wind power input. Because the solar wind power input includes the combined effects of almost all of the other parameters, we intend to analyze their respective effect now.

3.2. The Effects of the IMF B_z

The IMF B_z effect in the parameter of $d\Phi_{MP}/dt$ is reflected by the factor of $\sin^{8/3}(\theta/2)$, which implies that southward IMF can lead to more significant power input. Therefore, one may expect a high occurrence rate for the non-gap event under the southward IMF B_z. However, Figure 2c shows that the gap distribution (blue bars) and the gap occurrence rate (blue curve) show apparent bias toward the southward IMF B_z (i.e., at ~ −4 nT, as reflected by the relative occurrence rate). This result implies that the southward IMF statistically relates to weak auroral emission in the cusp region, which contradicts the expectation.

These IMF dependencies are well reflected in Figure 2d, which shows the high occurrence of the gap event from 90° to 270° clock angle.

3.3. The Effects of the IMF B_y and the Solar Wind Speed

Figures 2d and 2e indicate that the IMF B_y and the flow speed show outstanding effects in controlling the midday auroral emission. Their contributions to the solar wind power input of $d\Phi_{MP}/dt$ are reflected by the factor of $v^{4/3}B_T{}^{2/3}$. In order to investigate their respective effects in controlling the midday auroral emission, we carried out further analyses by dividing the non-gap events into different subsets based on the magnitudes of the IMF $|B_y|$ and of the solar wind speed.

First, we examined how the IMF varies with different solar wind speeds for non-gap events. Figures 3a and 3b show the IMF B_y distributions and the relative occurrence rates of the non-gap events observed with solar wind speed greater than 300, 400, 500, and 600 km/s, respectively. The relative occurrence rate is obtained by dividing the event number by the background number with the same solar wind speed ranges.

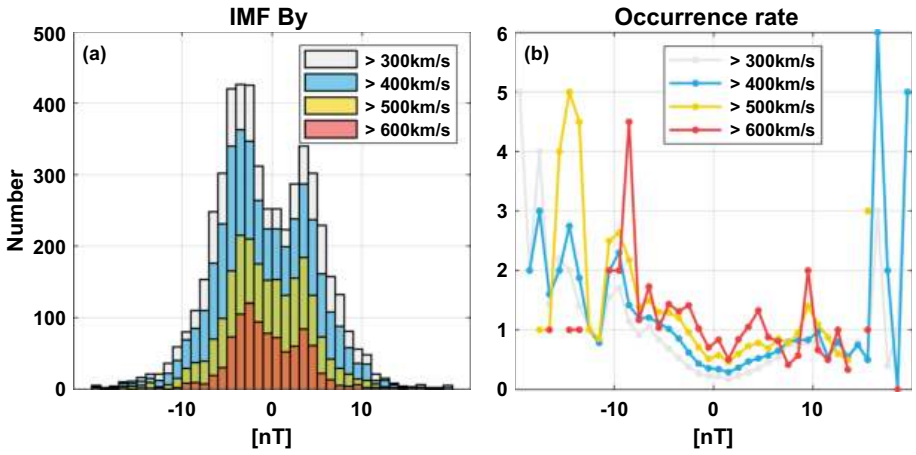

Figure 3. Overlapping of the IMF B_y distributions of the non-gap observed with solar wind speed greater than 300 (gray), 400 (blue), 500 (yellow), and 600 km/s (red) are shown in (a) and (b) gives the relative occurrence rates of the four subsets.

Figure 3a shows that with the solar wind speed increasing from 300 up to 600 km/s, a minimum non-gap occurrence is always observed near the IMF $B_y = 0$ nT. In Figure 3b, the minimum occurrence rate was observed for all of the speed ranges near the IMF $B_y = 0$ nT. These strongly imply that a weak IMF B_y is not favorable for the non-gap occurrence, even with high solar wind speed.

Second, we investigated how the solar wind speed distribution varied with the IMF B_y magnitude for the non-gap events and showed the results in Figure 4. Comparing the yellow and gray bars shown in Figures 4a–4c, we see that when the IMF $|B_y|$ becomes greater, the solar wind speed distribution shifts toward low value. This means that if the IMF B_y is strong, the requirement of high solar wind speed for the non-gap occurrence becomes less important. This effect is also reflected in Figures 4d–4f. We see that when the IMF $|B_y|$ increases from 3 to 5 nT, the distribution of the solar wind speed of non-gap events becomes more and more similar to the background distribution, which further implies that when the IMF B_y is strong, the solar wind speed becomes unimportant.

4. Summary and Discussion

By dividing the cusp auroras into weak (gap) and intense (non-gap) emissions, we noticed that the cusp auroral intensity is essentially controlled by the solar wind power input (Figure 2h). We further investigated the individual role of the main factors related to the solar wind input, including the IMF direction, the IMF magnitude, and the solar wind speed, in controlling the cusp auroral intensity. We found that the auroral midday gap events are predominantly observed under the southward IMF condition (Figure 2c), implying that the cusp auroral emission is generally weak under southward IMF. Although both the solar wind speed and the magnitude of IMF $|B_y|$ show a positive correlation with the cusp auroral emission (Figures 2b and 2e), an in-depth study (Figures 3 and 4) shows that the IMF $|B_y|$ magnitude is the critical factor in controlling the auroral intensity in the cusp region.

4.1. The Separate Contribution of V, B, and θ to the Cusp Auroral Intensity

Here, we call the auroras observed in the midday sector "auroras in the cusp region" or "cusp aurora" in brief. However, they may consist of the auroras that occurred in the low latitude boundary layer (LLBL), cusp, and plasma mantle. It is well known that the cusp and plasma mantle are on the open field lines. The LLBL in the midday sector was also suggested to be on the open field lines (Lockwood, 1997). So, we argue that the auroras considered in this work are all on the open field lines.

Figure 2h shows the auroral intensity in the cusp region is well controlled by the solar wind power input measured by a parameter of $d\Phi_{MP}/dt$. This parameter is determined by three factors, which are the solar

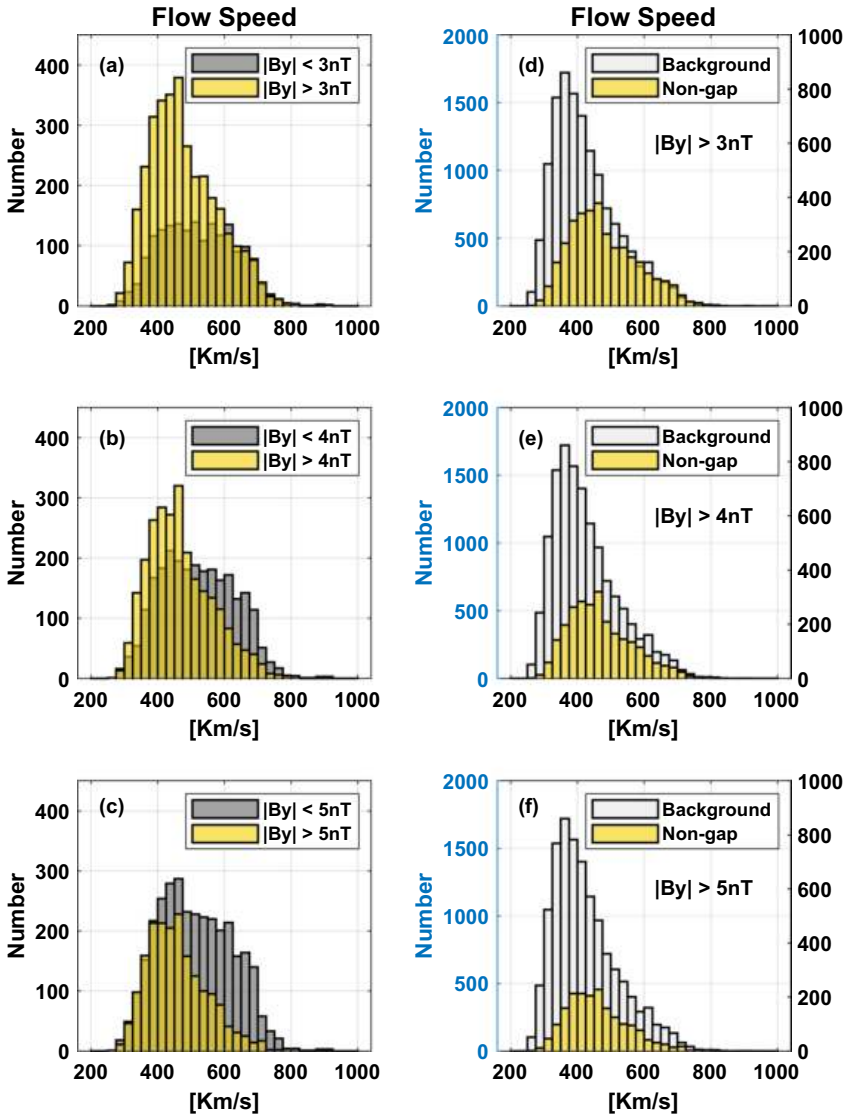

Figure 4. In the left column, yellow and gray bars show the solar wind speed distributions for the non-gap events observed with the IMF $|B_y|$ greater and less than a specific value (3, 4, and 5 nT), respectively. In the right column, in (d), (e), and (f), the shallow gray bars show the background solar wind speed distributions. The yellow bars show the solar wind speed distribution for the non-gap events observed with the IMF $|B_y|$ greater than 3, 4, and 5 nT, respectively.

wind flow speed, the IMF magnitude, and the IMF clock angle θ (Newell et al., 2007, 2009). The solar wind driving controlling the cusp auroral intensity has been noticed by Newell et al. (2009). Although previous studies reported that the auroral intensity in the midday sector is correlated with the solar wind speed (Yang et al., 2013), the IMF B_y (Trondsen et al., 1999), or the electric field produced by $V \times B_y$ (Hu et al., 2012), the separate contribution of these three factors on the dayside auroral intensity, especially in the cusp region, has not been revealed. We suggest that this study successfully distinguished the individual contribution of the three factors as follows.

In the parameter of $d\Phi_{MP}/dt = v^{4/3}B_T{}^{2/3}\sin^{8/3}(\theta/2)$, $\sin(\theta/2)$ implies that the solar wind power input is larger under southward IMF. It was also reported that the southward IMF contributes to the solar wind power input and the occurrence of auroral arcs (Lassen & Danielsen, 1978). However, we found that the occurrence of gap event (weak emission) is apparently higher under southward IMF (Figures 2c and 2d). Besides, it is worth noting that the non-gap event (intense emission) does not show any increase under southward IMF

(Figure 2c). These indicate that the cusp auroral intensity is statistically not well related to the magnetopause reconnection, as generally expected, but should be controlled by other processes.

Figures 2b and 2e show that the non-gap (intense emission) events prefer to occur with high solar wind speed and large IMF $|B_y|$. These are two factors that constitute the parameter of $d\Phi_{MP}/dt$, together with the IMF clock angle. Also, the product of these two factors produces a solar wind electric field in the north-south direction. In this study, Figure 3 shows that though the solar wind speed is as high as >600 km/s, the non-gap event still shows a minimum occurrence near the IMF $|B_y| = 0$. Further, Figure 4 shows that the effect of solar wind speed on the cusp auroral emission becomes less important when the IMF $|B_y|$ is greater. These results strongly indicate that the IMF $|B_y|$ is critical for the auroral emissions in the cusp region. Therefore, we suggest that the IMF $|B_y|$ may play a critical role in affecting the cusp aurora intensity by producing a north-south oriented solar wind electric field which is given as $V \times B_y$.

Figure 2e shows that the averaged solar wind speed for the non-gap events is predominantly higher than those for the gap events and higher than the background condition, indicating that the solar wind speed is also crucial for the cusp auroral intensity. We argue that this may reflect that only when the $V \times B_y$ electric field reaches a threshold can the cusp auroral intensity be enhanced.

4.2. What Role Does the $V \times B_y$ Electric Field Play?

Previously, it has been suggested that the north-south solar wind electric field produced by $V \times B_y$ can drive inter-hemispheric field-aligned currents by penetrating into the closed magnetosphere and thus increase the particle precipitation for producing the aurora (Hu et al., 2012; Kozlovsky et al., 2003). However, as pointed above, the auroras considered in this study are caused by particles from the LLBL, cusp, or plasma mantle, which are all on the open field lines. Therefore, we argue that driving an inter-hemispheric field-aligned current to penetrating the $V \times B_y$ electric field into the closed field line region cannot be the direct reason for explaining the critical role of the IMF $|B_y|$ on the cusp aurora intensity. Now we have to consider what role the $V \times B_y$ electric field plays.

As discussed above, because the non-gap event does not correlate with the southward IMF and the gap event show anti-correlation with the southward IMF, we suggest that the cusp aurora intensity may not reflect the activity level of magnetopause reconnection. Many previous studies suggested that the cusp auroras are produced by particles from the magnetosheath and are accelerated by Alfvén waves (e.g., Mende et al., 2016; Newell et al., 2005). Using Fast Auroral Snapshot (FAST) satellite observations, Hatch et al. (2017) examined the Alfvén wave-associated energy flux, Alfvén wave-driven broadband electron energy flux, and the broadband electron number flux for different IMF orientations. They found that the distributions of these parameters in the cusp region are all diminished under southward IMF, which are consistent with the weak aurora emission in the cusp region under the southward IMF, as shown in Figures 2c and 2d. Besides, Hatch et al. (2017) showed that when the IMF turns duskward or dawnward, the distributions of Alfvén wave-associated energy flux are enhanced in the cusp region. This is consistent with the bimodal distribution of the IMF B_y shown in Figure 2b. These results imply that the wave activity may be vital in affecting the auroral emissions in the cusp region, rather than the magnetopause reconnection.

Previous studies have presented much evidence to relate the cusp auroral intensity with wave activity. Korth et al. (2011) suggested that the solar wind Alfvén waves affect the magnetospheric cusp density and heat the cusp. Strangeway et al. (2000) suggested that Poynting flux is dominant in the particle energy input of the cusp region. Further, Knipp et al. (2011) suggested that both solar wind speed and the IMF B_y play a role in the dayside Poynting flux deposition. These factors related to Alfvén waves significantly affect the auroral intensity in this region.

Though the relationship between Alfvén wave activity and electric field has been investigated for years (e.g., Belcher et al., 1969; Varma et al., 2007), how the predominant north-south $V \times B_y$ electric field affects the Alfvén wave activity in the cusp region has not been clear yet. Based on the results above, we suggested the $V \times B_y$ electric field enhances the auroral intensity in the cusp region, most likely through enhancing the Alfvén wave activity. We stress that how the north-south electric field affects the Alfvénic wave activity is an open question and needs further investigation.

4.3. The Effects of the IMF B_x, Dynamic Pressure, and Solar Wind Density

It has been well recognized that high solar wind speed statistically corresponds to low solar wind density but can result in high dynamic pressure (Russell, 2013). As Figure 2e shows that the non-gap events are highly depend on the solar wind speed, we believe that the dependencies of the non-gap event on the dynamic pressure (Figure 2f) and solar wind density (Figure 2g) are self-consistent with the dependence on the solar wind speed.

In Figure 2a, based on the magnitude of $|B_x|$, we divide the IMF condition with the $|B_x| < 6.0$ nT and $|B_x| > 6.0$ nT the normal and radial IMF conditions, respectively. Please note that the radial IMF used here is an approximate classification but is not strictly consistent with previous definitions based on the IMF cone angle (e.g., Palmroth et al., 2015). For the normal IMF condition, Figure 2a shows that the non-gap occurrence rate increases with the magnitude of IMF $|B_x|$. We argue that this is also self-consistent with the dependence on the solar wind speed because a high solar wind speed generally leads to a larger IMF $|B_x|$ based on the Parker's solar wind spiral.

For the radial IMF condition, Figure 2a shows the non-gap occurrence rate is apparently higher than that of the gap event. We argue that this is well consistent with our suggestion about the wave activity deciding the cusp auroral intensity because the radial IMF condition can always lead to strong turbulence and wave activities in the dayside magnetosheath (e.g., Palmroth et al., 2015).

5. Conclusions

Based on DMSP/SUSSI observations from 2013 to 2017, we performed a systematic statistical study of weak and intense emissions in the cusp region. We found that (a) the auroral emission in the cusp region is generally weak under southward IMF, (b) high solar wind speed and large IMF $|B_y|$ contribute to intense auroral emission in the cusp region, and (c) the IMF $|B_y|$ magnitude plays a critical role in controlling midday auroral intensity. The clear statistical results inspire us to suggest that the north-south $V \times B_y$ electric field mainly generated by the IMF B_y significantly control the auroral power in the cusp region through the Alfvén wave activity in this region.

Data Availability Statement

All DMSP/SSUSI data used in this paper are available from https://ssusi.jhuapl.edu/data_products.

Acknowledgments
This work was supported by the National Natural Science Foundation of China (41831072, 42030101, 41974185, 41974193, and 41774174). We would like to thank Johns Hopkins University Applied Physics Laboratory for providing the DMSP/SSUSI auroral FUV data. We acknowledge the use of NASA/GSFC's Space Physics Data Facility's OMNIWeb service at https://cdaweb.gsfc.nasa.gov/index.html/.

References

Belcher, J. W., Davis, L., & Smith, E. J. (1969). Large-amplitude Alfvén waves in the interplanetary medium: Mariner 5. *Journal of Geophysical Research*, *74*(9), 2302–2308. https://doi.org/10.1029/ja074i009p02302

Dandekar, B. S. (1979). Relationship between the IMF, the midday gap, and auroral substorm activity. *Journal of Geophysical Research*, *84*(A8), 4413–4421.

Dandekar, B. S., & Pike, C. P. (1978). The midday, discrete auroral gap. *Journal of Geophysical Research*, *83*(A9), 4227–4236. https://doi.org/10.1029/ja083ia09p04227

Eather, R. H. (1981). Auroral motions under the dayside cusp. *Paper presented at IAGA Assembly, International Association of Geomagnetism and Aeronomy*, Edinburgh, UK.

Fasel, G. J., Lee, L. C., & Smith, R. W. (1995). *Dayside poleward-moving auroral forms: A brief review. Physics of the magnetopause*. American Geophysical Union (AGU). https://doi.org/10.1029/GM090p0439

Frank, L. A. (1971). Plasma in the Earth's polar magnetosphere. *Journal of Geophysical Research*, *76*(22), 5202–5219. https://doi.org/10.1029/ja076i022p05202

Fuselier, S. A., Frey, H. U., Trattner, K. J., Mende, S. B., & Burch, J. L. (2002). Cusp aurora dependence on interplanetary magnetic field B_z. *Journal of Geophysical Research*, *107*(A7), 1111. https://doi.org/10.1029/2001ja900165

Hardy, D. A., Holeman, E. G., Burke, W. J., Gentile, L. C., & Bounar, K. H. (2008). Probability distributions of electron precipitation at high magnetic latitudes. *Journal of Geophysical Research*, *113*, A06305. https://doi.org/10.1029/2007JA012746

Hatch, S. M., LaBelle, J., Lotko, W., Chaston, C. C., & Zhang, B. (2017). IMF control of Alfvénic energy transport and deposition at high latitudes. *Journal of Geophysical Research: Space Physics*, *122*, 12189–12211. https://doi.org/10.1002/2017ja024175

Heikkila, W. J., & Winningham, J. D. (1971). Penetration of magnetosheath plasma to low altitudes through the dayside magnetospheric cusps. *Journal of Geophysical Research*, *76*, 883–891. https://doi.org/10.1029/ja076i004p00883

Hu, Z.-J., Yang, H.-G., Han, D.-S., Huang, D.-H., Zhang, B.-C., Hu, H.-Q., & Liu, R.-Y. (2012). Dayside auroral emissions controlled by IMF: A survey for dayside auroral excitation at 557.7 and 630.0 nm in Ny-Ålesund, Svalbard. *Journal of Geophysical Research*, *117*, A02201. https://doi.org/10.1029/2011JA017188

Knipp, D., Eriksson, S., Kilcommons, L., Crowley, G., Lei, J., Hairston, M., & Drake, K. (2011). Extreme Poynting flux in the dayside thermosphere: Examples and statistics. *Geophysical Research Letters*, *38*, L16102. https://doi.org/10.1029/2011GL048302

Korth, A., Echer, E., Zong, Q.-G., Guarnieri, F. L., Fraenz, M., & Mouikis, C. G. (2011). The response of the polar cusp to a high-speed solar wind stream studied by a multispacecraft wavelet analysis. *Journal of Atmospheric and Solar-Terrestrial Physics*, *73*(1), 52–60. https://doi.org/10.1016/j.jastp.2009.10.004

Kozlovsky, A., Turunen, T., Koustov, A., & Parks, G. (2003). IMF By effects in the magnetospheric convection on closed magnetic field lines. *Geophysical Research Letters*, *30*, 2261. https://doi.org/10.1029/2003GL018457

Lassen, K., & Danielsen, C. (1978). Quiet time pattern of auroral arcs for different directions of the interplanetary magnetic field in the Y-Z plane. *Journal of Geophysical Research*, *83*, 5277. https://doi.org/10.1029/ja083ia11p05277

Lockwood, M. (1997). Relationship of dayside auroral precipitations to the open-closed separatrix and the pattern of convective flow. *Journal of Geophysical Research*, *102*, 17475–17487. https://doi.org/10.1029/97ja01100

Mende, S. B., Frey, H. U., & Angelopoulos, V. (2016). Source of the dayside cusp aurora. *Journal of Geophysical Research: Space Physics*, *121*, 7728–7738. https://doi.org/10.1002/2016JA022657

Meng, C.-I. (1981). Electron precipitation in the midday auroral oval. *Journal of Geophysical Research*, *86*(A4), 2149–2174. https://doi.org/10.1029/ja086ia04p02149

Meng, C.-I., & Lundin, R. (1986). Auroral morphology of the midday oval. *Journal of Geophysical Research*, *91*(A2), 1572–1584. https://doi.org/10.1029/ja091ia02p01572

Moen, J., Lorentzen, D. A., & Sigernes, F. (1998). Dayside moving auroral forms and bursty proton auroral events in relation to particle boundaries observed by NOAA 12. *Journal of Geophysical Research*, *103*(A7), 14854–14864. https://doi.org/10.1029/97ja02877

Newell, P. T., Sotirelis, T., Liou, K., Meng, C.-I., & Rich, F. J. (2007). A nearly universal solar wind-magnetosphere coupling function inferred from 10 magnetospheric state variables. *Journal of Geophysical Research*, *112*, A01206. https://doi.org/10.1029/2006JA012015

Newell, P. T., Sotirelis, T., & Wing, S. (2009). Diffuse, monoenergetic, and broadband aurora: The global precipitation budget. *Journal of Geophysical Research*, *114*, A09207. https://doi.org/10.1029/2009JA014326

Newell, P. T., Sotirelis, T., & Wing, S. (2010). Seasonal variations in diffuse, monoenergetic, and broadband aurora. *Journal of Geophysical Research*, *115*, A03216. https://doi.org/10.1029/2009ja014805

Newell, P. T., Wing, S., & Meng, C.-I. (2005). Spectral properties and source regions of dayside electron acceleration events. *Journal of Geophysical Research*, *110*, A11205. https://doi.org/10.1029/2005ja011264

Ober, D. M. (2014). The DMSP Space Weather Sensors Data Archive Listing (1982–2013) and File Formats Descriptions, *Air Force Research Laboratory Kirtland AFB, AFRL-RV-PS- TR-2014-0174, Accession Number*: ADA613822. 72 pp.

Palmroth, M., Archer, M., Vainio, R., Hietala, H., Pfau-Kempf, Y., Hoilijoki, S., et al. (2015). ULF foreshock under radial IMF: THEMIS observations and global kinetic simulation Vlasiator results compared. *Journal of Geophysical Research: Space Physics*, *120*(10), 8782–8798. https://doi.org/10.1002/2015ja021526

Russell, C. T. (2013). *Solar wind and interplanetary magnetic field: A tutorial. Space weather*. American Geophysical Union (AGU). https://doi.org/10.1029/GM125p0073

Russell, C. T., Fedder, J. A., Slinker, S. P., Zhou, X.-W., Le, G., Luhmann, J. G., et al. (1998). Entry of the POLAR spacecraft into the polar cusp under northward IMF conditions. *Geophysical Research Letters*, *25*, 3015–3018.

Sandholt, P. E. (1997). Dayside polar cusp/cleft aurora: Morphology and dynamics. *Physics and Chemistry of the Earth*, *22*(7–8), 675–684. https://doi.org/10.1016/s0079-1946(97)00195-x

Snyder, A. L., & Akasofu, S.-I. (1976). Auroral oval photographs from the DMSP 8531 and 10533 satellites. *Journal of Geophysical Research*, *81*(10), 1799–1804. https://doi.org/10.1029/ja081i010p01799

Strangeway, R. J., Russell, C. T., Carlson, C. W., McFadden, J. P., Ergun, R. E., Temerin, M., et al. (2000). Cusp field-aligned currents and ion outflows. *Journal of Geophysical Research*, *105*(A9), 21129–21141. https://doi.org/10.1029/2000JA900032

Trondsen, T. S., Lyatsky, W., Cogger, L. L., & Murphree, J. S. (1999). Interplanetary magnetic field by control of dayside auroras. *Journal of Atmospheric and Solar-Terrestrial Physics*, *61*, 829–840.

Varma, P., Mishra, S. P., Ahirwar, G., & Tiwari, M. S. (2007). Effect of parallel electric field on Alfven wave in thermal magnetoplasma. *Planetary and Space Science*, *55*, 174. https://doi.org/10.1016/j.pss.2006.07.007

Yang, Y. F., Lu, J. Y., Wang, J.-S., Peng, Z., & Zhou, L. (2013). Influence of interplanetary magnetic field and solar wind on auroral brightness in different regions. *Journal of Geophysical Research: Space Physics*, *118*, 209–217. https://doi.org/10.1029/2012JA017727

Zhang, Y., Meng, C.-I., Paxton, L. J., Morrison, D., Wolven, B., Kil, H., et al. (2005). Far-ultraviolet signature of polar cusp during southward IMFBz observed by TIMED/Global Ultraviolet Imager and DMSP. *Journal of Geophysical Research*, *110*, A01218. https://doi.org/10.1029/2004JA010707